Rheol Acta 34:221–234 (1995)

ORIGINAL CONTRIBUTION

Eric F. Brown
Wesley R. Burghardt
Hasan Kahvand
David C. Venerus

Comparison of optical and mechanical measurements of second normal stress difference relaxation following step strain

Received: 25 July 1994
Accepted: 9 January 1995

E.F. Brown · Prof. W.R. Burghardt (✉)
Department of Chemical Engineering
Northwestern University
Evanston, Illinois 60208, USA

H. Kahvand · Prof. D.C. Venerus
Department of Chemical Engineering
Illinois Institute of Technology
Chicago, Illinois 60616, USA

Abstract Relaxation of the second normal stress difference (N_2) following step strain of a concentrated monodisperse polystyrene solution has been studied using mechanical and optical rheometry. Measurements of normal thrust in a parallel plate geometry are corrected for strain inhomogeneity and combined with independent measurements of the first normal stress difference (N_1) to determine N_2. Optical experiments were performed using a novel configuration where flow birefringence data collected using multiple light paths within the shear plane are combined with the stress-optical law to determine all three independent stress components for shearing deformations. This technique eliminates end effects, and provides an opportunity to oversample the stress tensor and develop consistency checks of experimental data. N_2 is found to be nonzero at all accessible times, and relaxes in roughly constant proportion to N_1. This reflects nonaffine distribution of chain segments, even well within the regime of chain retraction at short times. Data collected with the two techniques are reasonably consistent with each other, and with results of previous studies, generally lying between the predictions of the Doi-Edwards model with and without the independent alignment approximation. The normal stress ratio $-N_2/N_1$ shows pronounced strain thinning in the nonlinear regime.

Key words Second normal stress difference – birefringence – tube model

Introduction

The goal of rheometry is a detailed characterization of the rheological response of complex materials to well defined deformation histories. In shearing flows, it is necessary to measure the shear stress and two normal stress differences to completely characterize the stress tensor. While there are well developed techniques for measuring shear stress and first normal stress difference, accurate measurements of the second normal stress difference are difficult (Walters, 1975). This is particularly true in transient flows, where transducer compliance effects encountered in mechanical rheometry can severely complicate normal stress measurements. At the same time, it is recognized that the behavior of the second normal stress difference can provide a sensitive test for constitutive models (Larson, 1988). Recent work further suggests that the second normal stress difference plays a critical role in determining the likelihood of viscoelastic instabilities at high Weissenberg number (Shaqfeh et al., 1992; Larson, 1992). These considerations provide ongoing motivation for developing techniques with the capability to accurately measure the second normal stress difference.

Study of the relaxation of stresses following step strain has been a particularly important experiment in the rheometry of polymers, since it generally facilitates a

Rheologica Acta, Vol. 34, No. 3 (1995)

separation of the time- and strain-dependent constitutive behavior of materials. Such experiments are usually restricted to shear stress measurements. There is ample evidence that the Lodge-Meissner relationship is quite generally satisfied (with the notable exception of very highly entangled polymer solutions and melts, see Larson et al., 1988), so that N_1 measurements in single step strain are in some sense redundant. The same cannot be said of the second normal stress difference, however. There are no general constitutive guidelines as to how N_2 should behave in step strain, and considerable variation is to be expected among different classes of materials (degree of entanglement, concentration, molecular weight distribution, chain architecture, etc.), and among various constitutive theories. To date, there has been only one report of measurements of N_2 in step strain, by Osaki et al. (1981), who characterized the ratio N_2/N_1 in a concentrated, entangled polystyrene solution using flow birefringence techniques.

Here, we describe measurements of N_2 during stress relaxation following step strain, using both mechanical and optical techniques. Several issues motivate this work. First, the central importance of step strain measurements and the second normal stress difference provides impetus for further development of a database of material behavior. Second, this problem provides a convenient vehicle to illustrate a new optical approach to the characterization of the full stress tensor in shearing flows. This technique provides advantages that i) only a single flow geometry is employed, ii) optical end effects are eliminated, and iii) it is possible to over sample the stress tensor and develop internal consistency checks in the data. With respect to the mechanical measurements, we note that recent strategies for measuring N_2 with mechanical rheometers have focused on specialized techniques using customized instruments. The measurements described here employ more readily available instrumentation (although it should be emphasized that considerable care must be employed in the experimental protocols) and consequently may be adopted by a broader range of experimentalists. Of course, we are also interested in the extent to which very disparate techniques will lead to self-consistent results. Finally, we have been motivated to consider N_2 relaxation in step strain experiments in light of some of the detailed predictions of fast time scale molecular relaxation processes in the context of the tube model.

Background

Definitions

Taking "1" to denote the shear flow direction, "2" the gradient direction, and "3" the neutral direction, the stress tensor in polymers subjected to a shearing deformation is given as:

$$\tau = \begin{pmatrix} \tau_{11} & \tau_{21} & 0 \\ \tau_{21} & \tau_{22} & 0 \\ 0 & 0 & \tau_{33} \end{pmatrix} . \tag{1}$$

Full characterization of the stress tensor requires measurements of the shear stress, τ_{21}, and first and second normal stress differences, $N_1 = \tau_{11} - \tau_{22}$ and $N_2 = \tau_{22} - \tau_{33}$.

For single step strain deformation, these material functions depend on time and the magnitude of the applied strain, γ. The nonlinear relaxation modulus $G(\gamma, t)$ is defined as:

$$G(\gamma, t) = \frac{\tau_{21}(\gamma, t)}{\gamma} . \tag{2}$$

In many polymers, the nonlinear relaxation modulus may, over certain time intervals, be factored into time- and strain-dependent terms:

$$G(\gamma, t) = h(\gamma) G(t) , \tag{3}$$

where $h(\gamma)$ is known as the damping function, and $G(t)$ is the linear relaxation modulus. In addition, most polymers have been found to obey the Lodge-Meissner relationship (1972) relating the shear stress and the first normal stress difference following a sudden step strain:

$$N_1(\gamma, t) = \gamma \tau_{21}(\gamma, t) . \tag{4}$$

In concentrated flexible polymers under modest deformations, the stress-optical rule (SOR) relates the anisotropic refractive index tensor to the stress tensor:

$$n = C\tau , \tag{5}$$

where C is the stress-optic coefficient (see, for instance, Janeschitz-Kriegel, 1983). The SOR provides the basis for rheo-optical measurements of stresses using the technique of flow birefringence.

Experimental approaches to N_2

Accurate characterization of the full stress tensor, and in particular the second normal stress difference, is a considerable challenge. N_2 is smaller in magnitude than N_1, and in the most widely used techniques to measure N_2, some combination of the two normal stress differences is actually measured, complicating the extraction of N_2. The first reliable mechanical measurements date back around 25 years. Ginn and Metzner (1969) combined

cone and plate and parallel plate flows to measure N_2 in steady shear flows. Around the same time, Olabisi and Williams (1972) and Miller and Christiansen (1972) pioneered the quantitative measurement of the radial pressure distribution in cone and plate flows, from which both normal stresses may be determined. More recently, this technique has been adopted and refined by Magda and coworkers (Magda et al. 1991a, b, 1993, 1994; Baek et al. 1993a, b). The radial distribution of normal pressure also provides the basis of a technique developed by Meissner et al. (1989) employing thrust measurements in cone and plate flow using sectored plates of various radii, which has been applied to steady shear flow of polymer melts. The tilted channel method implemented by Tanner (1970) is rare in that the measured fluid height is determined *only* by the action of N_2; however, it requires large quantities of test fluid, and is unsuitable for transient flows.

In steady shear flows of entangled polymers, N_2 has generally been reported to be in the range of -0.15 to -0.3 times N_1, with the normal stress ratio $\psi = -N_2/N_1$ relatively independent of shear rate. Recently, however, Magda et al. (1993, 1994) have shown that ψ is a strongly shear thinning function in steady shear flow. They suggest the constant values reported earlier may reflect polydisperse samples or samples whose concentration and molecular weights result in elastic instabilities in rotational rheometers at high Weissenberg numbers. Step strain experiments are able to probe large strains with less interference from viscoelastic instabilities, so nonlinear phenomena in N_2 might be more readily observed using this protocol. Studies of N_2 in time-dependent flows using mechanical tests have been carried out by Christiansen and Leppard (1974), Leppard and Christiansen (1975) and Ramachandran et al. (1985); in accord with their steady shear results, they found the normal stress differences basically tracked one another in both oscillatory flow and limited flow inception and relaxation experiments.

Transient normal stress measurements using mechanical techniques may be severely compromised by transducer compliance (see the section "Mechanical Rheometry"). This provides one of the motivations for the use of flow birefringence, where the noninvasive optical probe effectively decouples stress measurement from the flow cell, which may be made quite rigid. With flow birefringence, particular projections of the refractive index (and hence stress) tensor are selected by changing the light path relative to the shear flow direction. Measurements are typically conducted by sending the light down one of the three orthogonal axes defininig the shear flow. When light is sent down the vorticity (3) axis, the projection of the refractive index tensor onto the $1-2$ plane allows determination of τ_{21} and N_1. When light is sent down the shear gradient (2) axis, the measured birefringence is related to the *third* normal stress difference, $N_3 = N_1 + N_2$. Finally, it is possible to directly probe N_2 by sending the light down the flow (1) direction (Wales and Philippoff, 1973), but this geometry has not been widely employed, and is expected to be particularly susceptible to end effects, since N_2 is generally small in magnitude.

To fully determine the stress tensor using stress-optical methods, it is clear that at least two different projections of the refractive index tensor are required. Several investigators have combined measurements in the $1-2$ plane with measurements in the $1-3$ plane. This approach was followed by Philippoff (1961) in steady shear flow, by Osaki et al. (1981) in step strain measurements, and recently by Kannan and Kornfield (1992) in oscillatory shear flow.

Relation of N_2 to rheological constitutive theories

Integral constitutive equations provide a convenient means of describing the rheological behavior of entangled polymers and more recently have been in the simulation of complex flows of viscoelastic fluids (Luo and Tanner, 1986; Dupont and Crochet, 1988; Luo and Mitsoulis, 1990; Goublomme and Crochet, 1993; Bernstein et al., 1994; Feigl and Öttinger, 1994). Constitutive equations of the single-integral form can, for incompressible fluids, be written in the following general form

$$\tau_{ij}(t) = \int_{-\infty}^{t} \{\phi_1(t-\tau, I_1, I_2) C_t^{-1}(\tau)_{ij} + \phi_2(t-\tau, I_1, I_2) C_t(\tau)_{ij}\} d\tau \ , \tag{6}$$

where $C_t(\tau)_{ij}$ are the components of the Cauchy-Green tensor at time τ relative to the present time t; $C_t^{-1}(\tau)_{ij}$ is the Finger tensor; and ϕ_1 and ϕ_2 are material functions that depend on elapsed time $t-\tau$ and the invariants of $C_t(\tau)_{ij}$ given by:

$$I_1 = tr[C_t^{-1}(\tau)_{ij}] \ , \quad I_2 = tr[C_t(\tau)_{ij}] \ . \tag{7}$$

The well-known, phenomenological K-BKZ theory (Larson, 1988) is a special case of Eq. (6) in which the functions ϕ_1 and ϕ_2 are derived from an unspecified strain energy function. For fluids where time-strain factorability, Eq. (3), is applicable, the material functions can be written as:

$$\phi_i(t-\tau, I_1, I_2) = \frac{dG(t-\tau)}{d\tau} h_i(I_1, I_2) \ , \quad i = 1, 2 \ . \tag{8}$$

Even in cases when time-strain factorability is valid, determination of the damping functions h_i over the entire deformation space is a formidable task. To simplify

Rheologica Acta, Vol. 34, No. 3 (1995)

matters, the following restrictions on the damping functions h_i are commonly imposed

$$h_1(I_1,I_2) = (1+\beta)h(I_1,I_2) \ , \quad h_2(I_1,I_2) = \beta h(I_1,I_2) \ , \tag{9}$$

leaving the function $h(I_1,I_2)$ and the constant β to be determined using data from shear and extensional flow experiments.

For the step shear strain experiment described earlier, $I_1 = I_2 = 3+\gamma^2$, so that $h(I_1,I_2) = h(\gamma)$ and it is easy to show that Eqs. (6), (8) and (9) give Eq. (3). The apparent motivation for using the simplification in Eq. (9) is that the constant β gives the ratio N_2/N_1, which is generally regarded as small in magnitude and independent of strain. These assertions are based on the meager amount of N_2 data that have been reported and, in several of the cases (Luo and Tanner, 1986; Dupont and Crochet, 1988; Luo and Mitsoulis, 1990; Bernstein et al., 1994), the constant β is set equal to zero.

The absence of N_2 data for entangled polymer systems has negative implications on both the formulation and utilization of rheological constitutive equations. For example, the assumption that β is constant, or zero, has not in general been justified. Indeed, Goublomme and Crochet (1993) found that predicted extrudate swell ratios increased by nearly a factor of two as β was increased from -0.3 to 0; Feigl and Öttinger (1994) found that the calculated vortex size for flow in a 10:1 contraction increased monotonically as β was increased from -0.21 to 0. Furthermore, it is well known that the strain-dependent behavior of other material functions (i.e., shear viscosity) can have a significant effect on the stability and accuracy of complex flow simulations. Clearly, the absence of N_2 data, especially in step strain flows places severe restrictions on the advancement of complex flow modeling and simulation.

The tube model for polymer dynamics introduced by de Gennes and developed into a constitutive theory by Doi and Edwards has been extensively invoked as a *molecular* description of the linear and nonlinear rheology of entangled polymers (Doi and Edwards, 1986). For a nonlinear step strain, the initial deformation of the sample is presumed to result in a strictly affine deformation of chain segments, resulting in i) an uneven distribution of stretching along the chain's primitive path, and ii) an average stretching of the chain by a strain-dependent factor α. On a short time scale, τ_e, it is assumed that variations in local chain stretching are relaxed, leading to a deformed chain that is uniformly stretched beyond its equilibrium length. Two distinct processes then lead to a relaxation of the polymer stress. The first is retraction of the chain to its equilibrium length within the distorted tube, on a time scale τ_R. Retraction results in a substantial reduction of the stress levels in highly deformed polymers, and is responsible for the pronounced shear thinning character of the reptation model. Following retraction, the remaining stress is associated with the orientation of chain segments within the deformed tube; this is assumed to relax by the reptation mechanism ("disengagement") over a time scale τ_d.

In the basic Doi-Edwards model, it is assumed that retraction is an instantaneous process, which along with the independent alignment approximation leads to a constitutive equation of the form given in Eqs. (6) and (8). In step shear strain, time-strain factorability is predicted, with a damping function $h(\gamma)$ that is characterized by the extreme strain thinning behavior resulting from the retraction process (Doi and Edwards, 1986). Experimentally, monodisperse polymers typically show nonfactorable behavior at short times, which has been interpreted as a consequence of incomplete retraction. Extensions of the Doi-Edwards theory incorporating chain stretching have been proposed (Doi, 1980; Pearson et al., 1989), and seem able to capture the essence of short-time relaxation behavior in particular.

An affine shear deformations does not impart any anisotropy in molecular orientation in the 2–3 plane. Since flexible polymers are characterized by a proportionality of the polymeric stress to the second moment of the chain distribution function (the microscopic basis of the stress-optical rule), the initially affine shear deformation following application of a step strain should be characterized by a zero second normal stress difference. In the tube model, intrachain relaxation processes such as equilibration and retraction ultimately lead to a nonaffine distribution of chain segments. Attention is generally focused on how retraction relieves the strong chain stretching that accompanies affine deformation, since this leads to the most pronounced rheological consequence, shear thinning. However, a more subtle form of nonaffine deformation concerns the configuration tensor describing the distribution of segmental orientation characteristic of the reptation model. Depending on whether the independent alignment approximation is invoked, the Doi-Edwards model predicts a *nonzero* second normal stress difference, equal to either $-1/7$ or $-2/7$ of the first normal stress difference at small strains. The tube model thus predicts that N_2 should equal zero immediately following a step deformation, and then grow in magnitude to some finite value during the course of intrachain relaxation processes. Doi (1980) recognized this inconsistency between configuration tensors at early times, but did not pursue the issue since shear stress predictions are not sensitive to these subtle differences. Osaki et al. (1981) did not explicitly address this particular feature of the tube model, although their data suggest that N_1 and N_2 relax in constant proportion. Here, we are motivated to study the behavior of N_2 at the earliest times possible following application of a step strain.

Experimental

Materials

Experiments were performed on solutions of high molecular weight, low polydispersity polystyrene dissolved in tricresyl phosphate (TCP). Solutions were made independently for study by mechanical rheometry (IIT) and optical rheometry (Northwestern), using polystyrene purchased independently from Pressure Chemical Company, with a reported $M_w = 1.92 \times 10^6$, and polydispersity $M_w/M_n < 1.30$. The solvent TCP was purchased from Fisher Scientific and used as received. Appropriate amounts of solvent and polymer were weighed into a jar, whereupon several weeks were allowed to assure total dissolution of the polymer and homogenization of the solution. Both solutions studied had a polymer concentration of 12 wt%.

Mechanical rheometry

Venerus and Kahvand have studied the 12% polystyrene solution extensively, including measurements of the complex modulus, linear and nonlinear relaxation modulus in single step strain, and double step strains studying both shear (1994a) and normal stress relaxation (1994b). In order to measure the second normal stress difference, the strategy of combining parallel plate and cone and plate rotational geometries, applied to steady shear flow by Ginn and Metzner (1969), is employed.

In cone and plate flow with small cone angle Γ, an angular displacement Θ results in a very nearly homogeneous applied strain

$$\gamma = \Theta/\Gamma \ . \tag{10}$$

Measurement of the relaxation of torque $M(\gamma, t)$ and normal thrust $F(\gamma, t)$ following application of a sudden deformation allows direct measurement of the shear stress and first normal stress difference:

$$\tau_{21}(\gamma, t) = 3M(\gamma, t)/2\pi R^3 \ , \tag{11}$$

$$N_1(\gamma, t) = 2F(\gamma, t)/\pi R^2 \ , \tag{12}$$

where R is the radius of the cone and plate fixture. When an angular displacement is applied using parallel plates with gap H and radius R, the applied strain is inhomogeneous, and varies linearly with radial position in the gap,

$$\gamma(r) = \Theta r/H \ , \tag{13}$$

such that the strain applied at the outer radius of the fixture γ_R is given by:

$$\gamma(R) = \gamma_R = \Theta R/H \ . \tag{14}$$

Due to the inhomogeneous distribution of strain, and hence stress, the resulting torque and normal thrust are not simply related to the corresponding stresses. The inhomogeneity may be accounted for by performing experiments over a range of applied edge strain. Data for normal thrust may be used to determine the difference between N_1 and N_2 according to:

$$N_1(\gamma_R, t) - N_2(\gamma_R, t) = N(\gamma_R, t)\,[2 + \partial \log N(\gamma_R, t)/\partial \log \gamma_R] \ , \tag{15}$$

where $N(\gamma_R, t)$ is the normal thrust per unit area measured using parallel plates:

$$N(\gamma_R, t) = F(\gamma_R, t)/\pi R^2 \ . \tag{16}$$

Equation (15) may be derived along the lines of those used by Soskey and Winter (1984) who used torque data from parallel plates to determine $G(\gamma, t)$. By combining step strain relaxation measurements using cone/plate and parallel plate geometries, it is possible to determine N_2.

The finite stiffness of mechanical transducers can lead to anomalous normal force data. In order to obtain reliable data, the axial response time of the transducer, τ_A, must be much smaller than the mean relaxation time of the fluid, τ_M. Venerus and Kahvand (1994b) have discussed this issue extensively in the context of cone and plate measurements during step strain experiments on the same polystyrene solution studied here, which is determined to have a mean relaxation time of 15 s. In cone and plate flow, the characteristic normal force response time (associated with the squeeze flow that results from unwanted axial compliance) is:

$$\tau_A = 6\pi R \eta_0 / \Gamma^3 K \ , \tag{17}$$

where η_0 is the solution viscosity and K is the axial compliance of the transducer. The deleterious effect of compliance may be mitigated through the use of fixtures with small radius and relatively large cone angle. Venerus and Kahvand (1994b) show transient normal thrust data for four fixtures with τ_A ranging from 0.025 to 2.62 s. Provided $\tau_M/\tau_A > \sim 10^2$, excellent self consistency was found between different fixtures, indicating that compliance effects are negligible. In the case of parallel plate flows, the normal force response time is:

$$\tau_A = 3\pi R^4 \eta_0 / 8H^3 K \ . \tag{18}$$

At comparable edge separations $H \approx R\Gamma$, the effects of a squeeze flow are more severe in cone and plate geometries since the surface come much closer together. Consequently, it is relatively easier to avoid compliance effects in the

Rheologica Acta, Vol. 34, No. 3 (1995)

parallel plate geometry; all data reported here are taken under conditions where $\tau_M/\tau_A > \sim 10^2$.

Another consideration is the effect of finite strain rise time on normal stress signals. Venerus and Kahvand (1994b) report experiments in which the strain rise time was systematically varied from 50 to 150 milliseconds. All normal stress data were found to superimpose beyond a time of 0.25 s, indicating the data collected following this time are independent of the details of how the strain was applied.

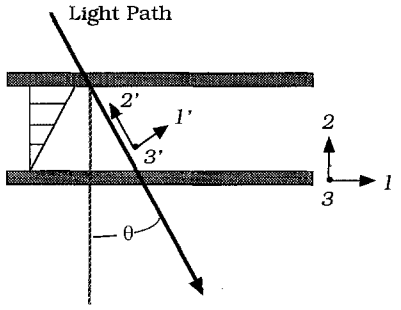

Fig. 1 Geometry used to compute birefringence as a function of optical path

Optical rheometry

Flow birefringence geometry

Optical approaches to the full refractive index tensor require measurements in at least two geometries, each interrogating different projections of $\boldsymbol{n}$. Past work has been restricted to situations in which light passes along the Cartesian axes used to define the shear flow geometry. Here, we explore an alternative strategy, where the projection of $\boldsymbol{n}$ is systematically varied by sending the light along a number of paths intermediate between the gradient (2) and shear flow (1) directions. A similar strategy was recently employed by Hongladarom and Burghardt (1994) to measure the full refractive index tensor in sheared liquid crystalline polymers. With the flexible polymer studied here, the stress optical rule allows a similar optical approach to probe relaxation of the full stress tensor following step strain.

Figure 1 shows a schematic of a shear flow geometry, including a light path within the shear plane at an angle θ with respect to the gradient direction. For modest values of the birefringence, the ordinary and extraordinary rays may be assumed to be collinear, and the polarization-dependent refractive index experienced by light passing through the sample may be obtained by rotating the refractive index tensor characteristic of a sheared polymer (Eqs. (1) and (5) above) to the primed (1′, 2′, 3′) coordinate frame:

$$\boldsymbol{n} = C \begin{bmatrix} \tau_{11}\cos^2\theta + \tau_{22}\sin^2\theta + \tau_{21}\sin 2\theta & -N_1\sin\theta\cos\theta + \tau_{21}\cos 2\theta & 0 \\ -N_1\sin\theta\cos\theta + \tau_{21}\cos 2\theta & \tau_{11}\cos^2\theta + \tau_{22}\sin^2\theta - \tau_{21}\sin 2\theta & 0 \\ 0 & 0 & \tau_{33} \end{bmatrix} . \tag{19}$$

With respect to this frame, birefringence is measured in the $1'-3'$ plane. Since the optical anisotropy in this plane is oriented along the $1'$ direction, the optical orientation angle χ is fixed at 0°, and the birefringence may be calculated as $\Delta n = n_{1'1'} - n_{3'3'}$, giving:

$$\Delta n = C[N_1\cos^2\theta + \tau_{21}\sin 2\theta + N_2] . \tag{20}$$

Following step strain relaxation, the birefringence will decay with time as the stresses in the sample relax.

Equation (20) shows the birefringence varies as a function of θ and includes contributions from all three material functions. When $\theta = 0°$ or 90°, the birefringence reflects N_3 or N_2, respectively, recovering two traditional flow birefringence geometries; at intermediate angles, the shear stress also contributes. To determine all three material functions, three independent values of θ are required. Like most methods for determining N_2, the present technique ultimately requires manipulation of large quantities to extract the desired small quantity. However, in this case, it is possible to collect extra data by using additional light paths, allowing a check of internal self-consistency in the measurements and yielding some objective measure of the degree of precision possible with this technique. An additional advantage of this approach is that it is possible to fully determine $\boldsymbol{n}$ with measurements at the same point in a single flow cell, in a geometry where there are no end effects associated with undesired flow disturbances along the light path (encountered with measurements in the $1-2$ and $2-3$ planes).

Flow cell

The flow cell is built around a pair of specially fabricated prisms (Kappler Crystal Optics) illustrated in Fig. 2a. Faces are cut at 0°, 30°, and 60° which allow light to pass through the sample with minimal refraction. The relative contribution to N_2 to the birefringence signal increases with θ, so steeper angles enhance the ability to extract accurate N_2 values. The sample is sandwiched between the two prisms, and shear flow is generated by displacing one relative to the other. Changing the direction of the flow is equivalent to experiments at −0°, −30°, and −60° (of course, experiments at ±0° should be identical), so this design allows oversampling of the stress tensor. The

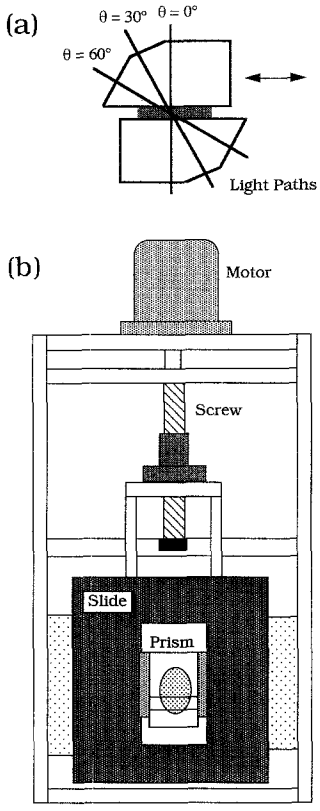

Fig. 2 Schematic diagram of flow cell. a) Prisms used as optical windows, showing faces cut to facilitate multiple light paths. b) Illustration of flow cell construction

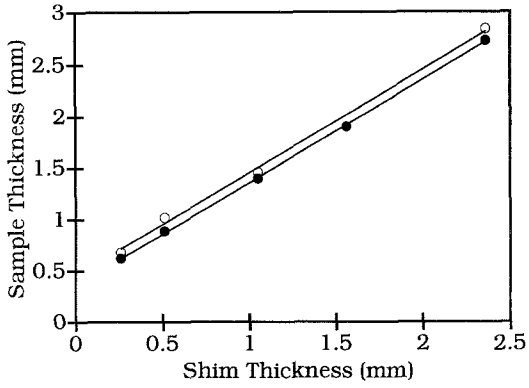

Fig. 3 Sample thickness as a function of spacer thickness. Closed symbols represent thickness measured directly by insertion of precision gauges, open symbols represent thicknesses inferred from the ratio of N_1 to τ_{21}, assuming the validity of the Lodge-Meissner relationship (see Fig. 11). Lines drawn with slope of unity

prisms are glued to aluminum holders, which in turn are mounted onto a precision linear motion stage (Parker-Daedal), driven through a pre-loaded ball screw and nut by a microstepping motor (Compumotor); Fig. 2b shows an illustration of the flow cell construction.

Since the prisms allow only a restricted range of linear motion, the sample gap is adjusted to facilitate a wide range of shear strains; larger strains employ smaller gaps. Precision shims are used to vary the thickness in a well-defined fashion, but it proved difficult to accurately measure the thickness in the assembled flow cell. A sequence of precision gauges of known diameter were slid between the two prisms to measure the sample thickness as a function of shim thickness; results are indicated by the solid symbols in Fig. 3, where the line is drawn with a slope of 1. Given the gap, the linear displacement L required for a given strain was converted to an angular displacement with the screw pitch, and applied by the motor.

Optical train

Birefringence was measured using a polarization modulation technique as described by Frattini and Fuller (1984). Light from a HeNe laser is polarized with a Glan-Thompsen calcite polarizer oriented along the flow direction ($\chi = 0°$), and then passed through a photoelastic modulator (PEM, Hinds Instruments, carrier frequency 42 kHz) oriented at 45°. The flow cell was mounted on a large precision rotation table positioned so the same portion of the sample was illuminated as the flow cell was rotated relative to the light beam. Mounting of the prisms resulted in a small parasitic birefringence oriented along the flow axis of the cell; a Babinet-Soleil compensator (Oriel) was positioned immediately behind the flow cell to cancel the optical effect of the static birefringence. The light beam then passed through a polarizer oriented at 45°, and light intensity was measured using a high speed photodiode (Hinds). The measured light intensity includes *dc* and harmonic components. By setting the modulation amplitude A such that $J_0(A) = 0$, the *dc* component is independent of any anisotropic optical properties of the sample, and the light intensity takes the form:

$$I = \frac{I_0}{4}[1 + 2J_1(A)\sin\delta\sin\omega t + \text{higher harmonics}] \,. \tag{21}$$

$J_1(A)$ is treated as a calibration constant, determined using a sample of known optical properties. A low pass filter measures the *dc* component of the light intensity, while a lock-in amplifier is used to extract the first harmonic at the modulation frequency, ω. Taking a ratio of these quantities allows determination of the retardance of the sample:

$$\delta = \frac{2\pi\Delta nd}{\lambda} \,, \tag{22}$$

from which the birefringence may be calculated using the known wavelength, λ, and optical path length, d. Note that this design of optical train allows unambiguous

determination of the sign of Δn, important in the context of the present technique. Application of the strain and subsequent data acquisition are computer controlled; full details of the experimental procedures may be found in Brown (1993).

The flow cell prisms are made out of BK7 optical glass with a refractive index of 1.5175, while the solution's refractive index was measured to be 1.566 using an Abbe refractometer. As a result of the mismatch, the laser beam is slightly refracted at the prism/solution interface. Snell's law gives the following propagation angles within the sample: $\theta = \pm 0°$, $\pm 29.0°$, and $\pm 57.2°$. These values are used when calculating the optical path length d for the different propagation directions for use in Eq. (22), and also when analyzing the data to extract the material functions according to Eq. (20). In addition, refraction through an oblique interface may also be accompanied by polarization effects. These are easily incorporated into the optical analysis through the appropriate Fresnel transmission coefficients. For the minor mismatch in refractive index here, however, refraction has virtually no impact on the light polarization state.

Results

Mechanical results

Figure 4 shows measurements of the nonlinear relaxation modulus of the 12% polystyrene solution as measured in cone and plate flow. The behavior is typical of well entangled solutions of linear, monodisperse polymers. As $\gamma \to 0$, the data superimpose to given the linear relaxation modulus, $G(t)$. As strain increases, pronounced strain softening is observed, where $G(\gamma, t)$ is seen to decrease by over an order of magnitude. At long times, all nonlinear modulus curves are parallel, and $G(\gamma, t)$ may be factored into time and strain-dependent terms, as in Eq. (3). Shifting the curves in Fig. 4 allows determination of the mechanically measured damping function, $h(\gamma)$, represented by solid triangles in Fig. 5. Also shown are the damping function predictions of the Doi-Edwards model, with and without the independent alignment approximation. As has been typically observed in similar system, the Doi-Edwards model provides an excellent description of the nonlinear viscoelasticity measured in step strain, including the severe strain thinning seen experimentally.

At short times, the relaxation modulus clearly is not factorable, and there are enhanced stress levels relative to the Doi-Edwards prediction. As discussed earlier, it is believed that this extra stress results from partial chain stretching associated with incomplete retraction. Factorable behavior is seen for times greater than around 3 s, suggesting that retraction is still occurring at all times less than 3 s. Actually, this time scale is rather longer than estimates of τ_R believed to be associated with Rouse-type relaxation of the entire chain within the tube, a fact that has been discussed previously by Osaki et al. (1982). It would appear that intrachain relaxation processes are somewhat more sluggish than basic scaling arguments suggest.

To make measurements of N_2 following the strategy described earlier, normal thrust measurements in cone and plate and parallel plate flows must be combined. Figure 6(a) shows normal thrust data measured with parallel plates. To generate these data, step strain relaxation experiments were conducted at a series of edge strain γ_R, and the data were cross-plotted at discrete time intervals as a function of strain. As seen in Eq. (15), it is necessary to differentiate these data as a function of strain. To facilitate this process, the data were fit to the

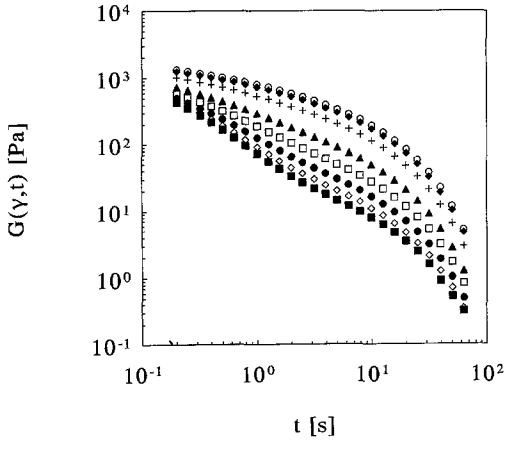

Fig. 4 Nonlinear relaxation modulus as a function of strain, measured mechanically in cone and plate flow. Strains of: ≤0.5 (○), 1.0 (◆), 2,0 (+), 4.0 (▲), 6,0 (□), 8.0 (●), 10.0 (◇), 12.0 (■)

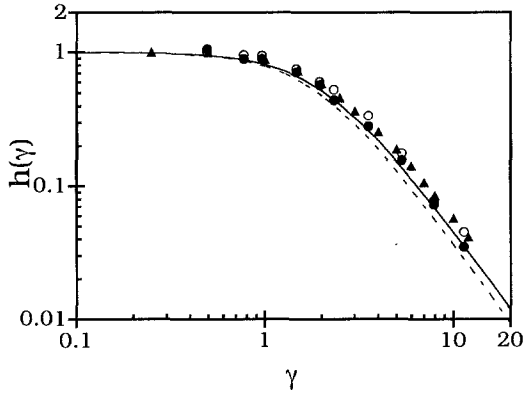

Fig. 5 Shear damping function, $h(\gamma)$, vs strain, measured mechanically (▲), and optically using data from ±30° experiments (○) and ±60° experiments (●). Predictions of Doi-Edwards model shown with (solid line) and without (broken line) the independent alignment approximation

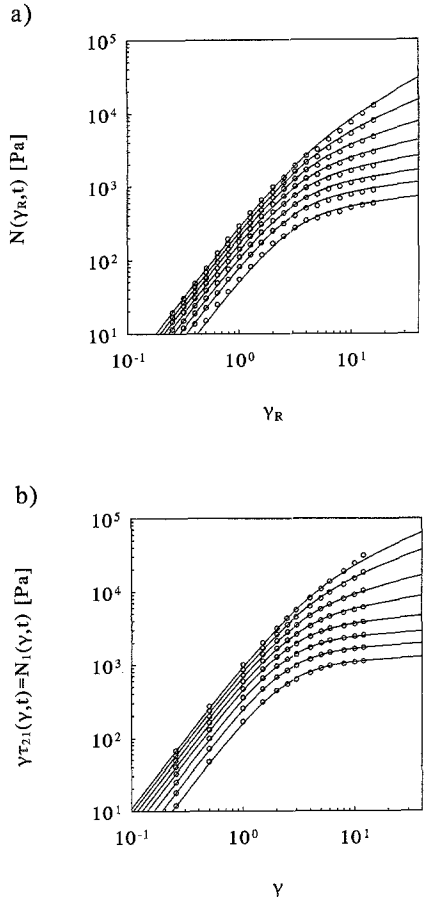

Fig. 6 Mechanical normal stress measurements following step strain. a) Normal thrust per unit area measured in parallel plate geometry. b) Strain time shear stress as measured in cone and plate flow. Solid lines are fit to data using Eq. (23). From top down, data sets correspond to times of 0.40, 0.63, 1.0, 1.6, 2.5, 4.0, 6.3, and 10 s

following strain-dependent function having a sigmoidal form suggested by Soskey and Winter (1984):

$$N(\gamma_R, t) = \frac{c(t)\gamma_R^2}{1+a(t)\gamma_R^{b(t)}}, \tag{23}$$

where $a(t)$, $b(t)$ and $c(t)$ were adjusted to data obtained at a particular time, t. Beyond having the appropriate quadratic strain-dependence at small strain amplitudes, we do not ascribe any particular significance to this functional form, and adopt Eq. (23) solely on the basis of its ability to accurately represent the experimental data in Fig. 6(a). In subsequent manipulations, Eq. (23) is used in place of the experimental data. Based on the scatter of the data around the curves and the expected accuracy of the normal force transducer, this representation of the data should be accurate to within ±5%. Using Eq. (15), $N_1(\gamma_R, t) - N_2(\gamma_R, t)$ was determined from these parallel plate measurements.

To extract N_2, it is necessary to have an independent measure of N_1 relaxation during step strain. Venerus and Kahvand (1994a, b) have studied shear and normal stresses of this sample extensively in cone and plate flow, and in particular note that the Lodge-Meissner relationship is satisfied. Since shear stress measurements are subject to fewer artifacts than normal stress measurements, we use shear stress measurements in cone and plate flow, in conjunction with the Lodge-Meissner relationship, to produce the values of $N_1(\gamma, t)$ shown in Fig. 6(b), for the same times at which $N_1 - N_2$ is evaluated from parallel plate relaxation data. These data may also be very well fitted to an equation of the same form as (23), again to an accuracy within ±5%.

Finally, subtracting the two results enables isolation of the second normal stress difference. Figure 7 shows the results, in which the ratio $-N_2/N_1$ is plotted as a function of strain, evaluated at the discrete time intervals used in the analysis. As is characteristic of similar techniques, relative errors are considerably amplified by the subtraction of two large quantities to extract the smaller N_2. Using error estimates of ±5% for the representation of data in Fig. 6 with Eq. (23), error bars may be determined for the normal stress ratio. For the sake of clarity, only a few representative error bars are shown in Fig. 7. As considerable manipulation of data is required to reach these results, it is not surprising that there should be a fair amount of scatter in the data, and in fact the small strain limit of N_2/N_1 ranges from −0.15 to −0.25. Nevertheless, the data do show some important characteristics. First, the normal stress ratio is clearly seen to decrease with increasing strain for all measurement times. Second, within the accuracy possible with this technique, there are

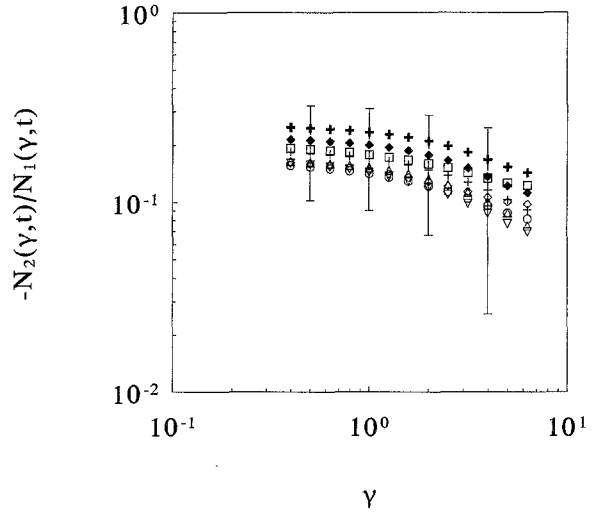

Fig. 7 Normal stress ratio $-N_2/N_1$ as a function of applied shear strain, measured mechanically. Symbols indicate time following application of step strain: 0.40 s (+), 0.63 s (△), 1.0 s (○), 1.6 s (▽), 2.5 s (◇), 4.0 s (□), 6.3 s (♣), 10 s (◆), with representative error bars)

no systematic changes in the normal stress ratio with time. We will return to these points and make comparisons of these data with the Doi-Edwards model once the analogous optical data have been presented.

Optical results

Figure 8 presents typical birefringence relaxation curves measured along the six possible light paths in the optical flow cell: ±0° (degenerate), ±30° and ±60°. To understand these curves, it is necessary to recall that polystyrene has a negative stress optical coefficient. Thus, the curves measured with forward and backward applied strain at normal incidence (±0°) show a negative birefringence, corresponding to a *positive* third normal stress difference. As expected, there is excellent agreement beween these two curves. Changing the light path away from the normal direction has two effects. The relative contributions of N_1 and N_2 to the measured birefringence change, and at the same time, the shear stress contributes to Δn. As seen in Eq. (20), the shear stress contribution changes sign with θ; at the modest strain levels in Fig. 8, the sign change of the shear stress contribution is sufficient to change Δn from negative to positive values for the −30° and −60° experiments (hence the importance of using an optical technique sensitive to the sign of the birefringence).

To extract the relaxation behavior of the individual stress components, the following procedure was used. First, the data measured at ±0° were averaged to yield N_1+N_2. If data taken at +30° and −30° are subtracted, the normal stress contributions to the birefringence cancel one another, so that the shear stress may be isolated. If they are added, the shear stress contributions cancel one another, and the result reflects contributions from N_1 and N_2, but with a different relative weighting from the 0° data. By combining the 30° data with the 0° data, it is thus possible to extract all three individual shear material functions. A similar procedure may be followed with the data at ±60°, to obtain an independent measure of the shear stress, and, again in combination with the 0° data, a measure of N_1 and N_2 individually. We adopt a shorthand notation of "30°" to designate normal stress components measured using the 30° data in combination with the 0° data.

Figure 9 shows the results of these manipulations using the birefringence data shown in Fig. 8. At a strain $\gamma = 1$, the shear stress and normal stress should be identical, as is very nearly observed. The second normal stress difference is found to be negative, and smaller in magnitude than N_1, as expected. Comparing parts (a) and (b), there is generally rather good consistency between the stresses obtained from the different optical data, although the normal stresses tend to be noisier when extracted from the 30° data. This is to be expected, since there is relatively less contrast between the contributions of N_1 and N_2 to the birefringence when combining 0° and 30° data than when combining 0° and 60° data (Eq. (20)).

Figure 10 compares the two shear stress relaxation curves measured optically with mechanical measurements at this strain level. The optical shear stress curves are very nearly indistinguishable, and there is excellent agreement

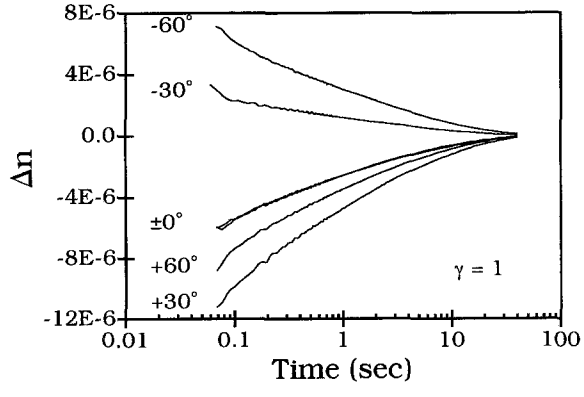

Fig. 8 Birefringence as a function of time following application of shear strain $\gamma = 1$, using indicated light path angle

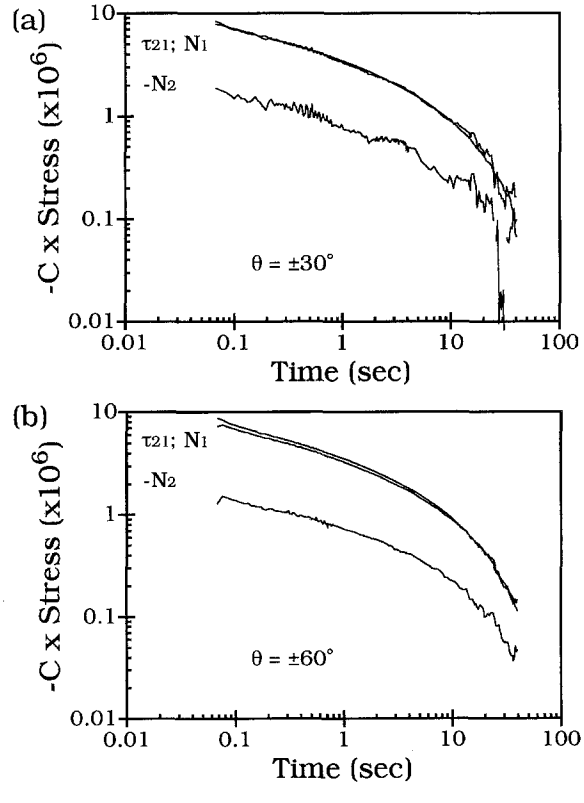

Fig. 9 Shear stress, and first and second normal stress difference relaxation following application of a shear strain $\gamma = 1$. Stresses calculated from optical data presented in Fig. 8 at 0° in conjunction with data at a) ±30°, and b) ±60°

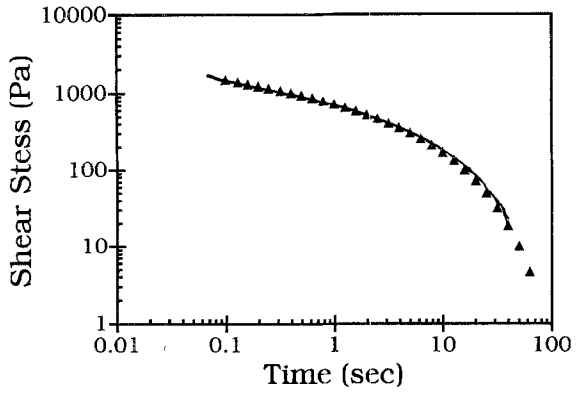

Fig. 10 Comparison of optical and mechanical measurements of shear stress relaxation following shear strain $\gamma = 1$. The symbols represent the mechanical measurements, while the two curves are optical results using data from $\pm 30°$ and $\pm 60°$

with the mechanically measured modulus, particularly in light of the fact that measurements were performed on solutions prepared independently. From these data, a stress-optical coefficient $C = -5 \times 10^{-9}\,\mathrm{Pa}^{-1}$ was determined, in good agreement with previously reported values in solutions of PS in TCP (for instance Larson et al. (1988)). Optical measurements of the nonlinear relaxation modulus yielded similar results to the mechanical data in Fig. 4 (Brown, 1993). Factorability is observed at long times, and there is excellent agreement between the mechanically and optically determined damping function, seen in Fig. 5.

Figure 11 (a) shows an experimental test of the Lodge-Meissner relationship for the optical data at a strain $\gamma = 1$. The ratio N_1/τ_{21} is indeed found to be constant during the relaxation, until long times where the data become very noisy due to weak signals. Values derived from the 30° and 60° optical data agree reasonably well with one another, but are slightly below the theoretically predicted value of 1. Figure 11 (b) shows the Lodge-Meissner ratio averaged over time $0.1 \le t \le 10$ s, plotted as a function of the applied strain. The negative deviations become more pronounced at higher strains, where thinner shims are employed. Particularly since this solution is known to obey the Lodge-Meissner relationship, this suggests a systematic error in sample thickness. By grouping the data in Fig. 11 (b) according to which shim was used, a "true" strain (and hence sample thickness) was determined by enforcing the Lodge-Meissner rule (Brown, 1993). Figure 3 shows the resulting thicknesses represented by open symbols. The method originally used to measure the prism spacing seems to systematically underestimate the thickness by a small amount. In Figs. 5 and 12, corrected strain values are used in reporting the strain. A small error in thickness also will result in slightly erroneous values of birefringence being extracted from the optical data using Eq. (22); however, these errors would

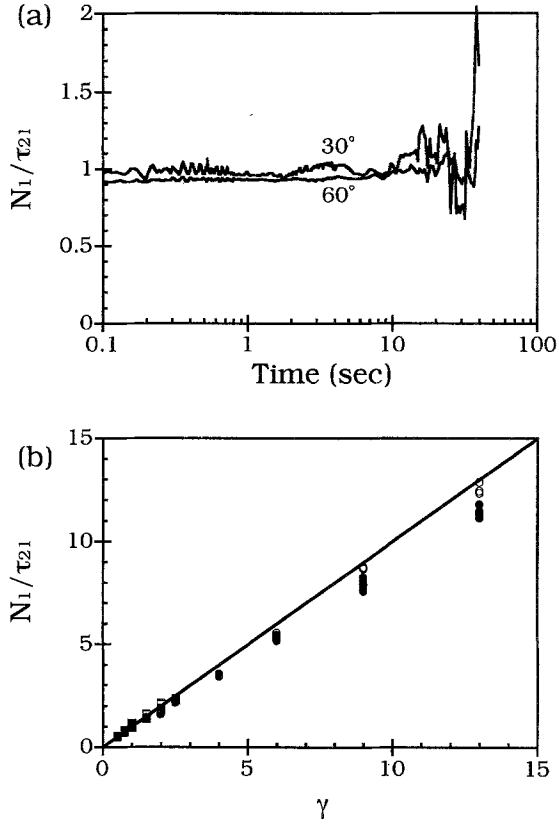

Fig. 11 Test of Lodge-Meissner relationship using optical technique. a) Ratio of first normal stress difference to shear stress as a function of time following strain $\gamma = 1$. b) Ratio of first normal stress difference to shear stress, averaged from $0.1 \le t \le 10$ s, as a function of the supposed magnitude of the applied strain. Different symbols correspond to different shim thickness

by and large be absorbed into the stress-optical coefficient. In particular, the dimensionless ratio $-N_2/N_1$ is extracted from the optical data in such a way that it is completely independent of any uncertainty in thickness.

Figure 12 shows the time dependence of the normal stress ratio at an applied strain $\gamma = 1$; qualitatively similar results are seen at other strain levels. There is once again reasonable self consistency between the 30° and the 60° data, although there is a higher noise level associated with the extraction of N_2. The degree of self consistency observed by comparing the 30° and 60° degree data provides an indication of the precision with which measurements can be made using this technique. Multiple realizations of the entire experimental sequence allows the reproducibility of the normal stress ratio to be tested. For a strain $\gamma = 1$, 30° data yield a standard deviation of 16.3% around the mean value for times between 0.1 to 1 s, which grows to 32.2% for times between 1 and 5 s. For 60° data, the corresponding numbers are 4.7 and 6.9%; these values are illustrated as representative error bars on the optical data in Fig. 12. At longer times, the

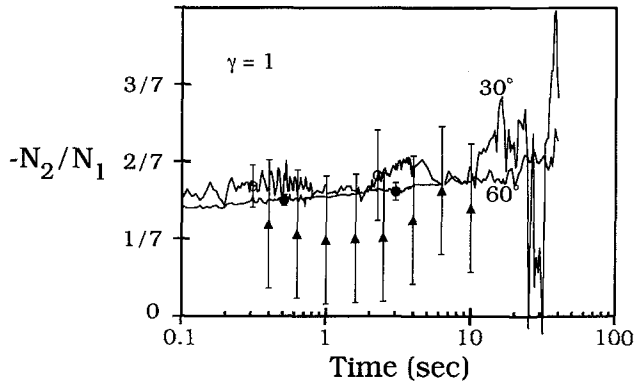

Fig. 12 Normal stress ratio, $-N_2/N_1$ as a function of time following strain $\gamma = 1$. Mechanical measurements, with error bars (▲). Lines give optical measurements, designated 30° (○) and 60° (●); error bars on optical measurements indicate degree of reproducibility in multiple experiments; see text

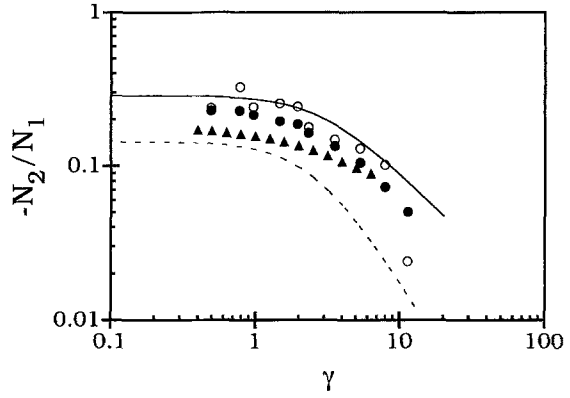

Fig. 13 Normal stress ratio, $-N_2/N_1$, averaged from $0.1 \leq t \leq 10$ s, as a function of strain; measured mechanically (▲), and optically using data from ±30° (○) and ±60° (●) experiments. Predictions of Doi-Edwards model shown with (solid line) and without (broken line) the independent alignment approximation

data become less reproducible due to weak signals. It is not surprising that the 60° data are considerably more robust, since there is significantly greater sensitivity to contributions from N_2 in the ±60° experiments (see Eq. (20)). Experiments at higher strain levels give better reproducibility, due to both higher signal levels and increased relative importance of normal stresses in the birefringence signal.

Symbols in Fig. 12 give the corresponding mechanical measurements at this strain level. This representation of the data also demonstrates that the mechanical results show no systematic changes with time within experimental error. The optical data, however, show a reproducible slight increase in the magnitude of the normal stress ratio throughout the course of the relaxation. For instance, the 60° data exhibit an increase in $-N_2/N_1$ from 0.21 at 0.2 s to 0.24 at 5 s. This level of increase is typical of data at other strains (Brown, 1993). We typically find that the optical method yields somewhat higher values of the normal stress ratio than the mechanical technique.

Figure 13 summarizes optical measurements of the normal stress ratio as a function of strain, in which data are averaged over times from 0.1 to 10 s. For inclusion in this figure, the mechanical data have been similarly averaged. Finally, we include predictions of the Doi Edwards model with and without independent alignment (with corresponding zero strain predictions of 2/7 and 1/7, respectively). As anticipated from Fig. 12, the optical data give systematically larger values of the ratio. Generally speaking, the data lie between the two predictions, with the mechanical data closer to the rigorous predictions and the optical data in closer agreement with the independent alignment predictions. In addition, the optical data seem to exhibit a greater degree of shear thinning than the mechanical data, which seems to be in better qualitative agreement with the model predictions. Comparing the optical results at 30° and 60°, the 30° data generally yield a larger value of the ratio. However, the 30° results exhibit a more erratic strain dependence than that derived from the 60° data. Since steeper angles enhance sensitivity to N_2 (see error bars in Fig. 12), we attach more significance to the 60° results. Bearing this in mind, the optical data suggest a low strain asymptote of $(-N_2/N_1)_0 = 0.23$, while the mechanical data yield $(-N_2/N_1)_0 = 0.17$.

Discussion

The data in Fig. 13 are in good qualitative agreement with the observations of Osaki et al. (1981). The reasonable self-consistency of the mechanical and optical data and the agreement with the results of Osaki et al. demonstrate that both techniques employed here are suitable for measuring N_2 relaxation following step strain. Since the mechanical method uses standard instrumentation, it may facilitate study of the second normal stress difference in step strain for a wider class of materials than is possible with more highly customized techniques, such as the new optical approach described here. As is expected, the data manipulation required by the mechanical technique makes it quite susceptible to small errors. Nevertheless, it correctly captures some important qualitative characteristics such as shear thinning of the normal stress ratio. At the same time, the optical method appears to be quite robust, particularly for the case of the ±60° data. Both data sets generally lie between the rigorous and approximate predictions of the Doi-Edwards model, typical of a wide range of results in the literature. It is interesting that the *mechanical* data in the present study are closer both to the rigorous Doi-Edwards predictions and to the birefringence results of Osaki et al. (1981), while the present

optical measurements are closer to the independent alignment prediction.

Although much emphasis has been placed on the low strain (or shear rate) limit of N_2/N_1 (Hassager, 1985) it seems unlikely that experiments conducted with a variety of techniques will exhibit sufficient consistency to definitively resolve this particular issue. Nonlinear viscoelastic effects on the normal stress ratio do, however, show clear trends. Consistent with recent experiments by Magda et al. (1993, 1994), our measurements show shear thinning of the ratio $-N_2/N_1$, in agreement with the Doi-Edwards model predictions. In light of this evidence, the commonly adopted form for the K-BKZ theory given in Eq. (9) is inadequate for these well characterized solutions, and perhaps more generally for entangled linear polymers. This has particular significance since the normal stress ratio does have substantial impact on the predictions of numerical simulations based on integral models (see the section "Relation of N_2 to rheological constitutive theories").

In Fig. 12, the normal stress ratio is seen to be nearly constant throughout the stress relaxation process, including the earliest times for which reliable data may be acquired using these methods. While an increase in the magnitude of the ratio is qualitatively consistent with a transition from affine to nonaffine behavior, the strongly nonzero N_2 observed at short times indicates that the distribution of chain orientation is nonaffine during the *entire* observable relaxation process, including times well within the regime where nonfactorability of the relaxation modulus indicates retraction is still occurring. Care must be taken to distinguish between subtle nonaffine effects at short times ($N_2 \neq 0$) and the grossly nonaffine chain stretching present once retraction has acted to reduce tension along the primitive path ($h(\gamma) \ll 1$). Apparently, the starting point of a rigorously affine deformation in the tube model description of step strain becomes quickly irrelevant due to extremely rapid equilibration of chain stretching on time scales that cannot be resolved here. For *practical* purposes, the instantaneous response of physically entangled polymers looks very much like that of crosslinked rubbers, where it has long been appreciated that the Mooney-Rivlin equation with nonzero C_2 (presumably reflecting nonaffine deformation of network strands; see Wagner, 1994) performs better than the classical affine phantom network model.

Summary and conclusions

Measurements of second normal stress difference relaxation following step strain have been successfully performed using mechanical and rheo-optical methods. The mechanical data demonstrate that such measurements may, with care, be performed using relatively standard rheological testing equipment and protocols, and yield important qualitative information such as strain thinning of the normal stress ratio. The optical experiments have utilized a novel configuration in which multiple light paths within the shear flow plane are used to interrogate the full stress tensor. Since the stress tensor is oversampled, this allows internal consistency checks on stress-optical measurements of N_2 for the first time. Results from both techniques are in reasonable agreement with previously published data, and generally lie between the predictions of the Doi-Edwards model with and without independent alignment. In particular, the normal stress ratio $-N_2/N_1$ shows considerable strain thinning. The normal stress ratio is nearly constant with time throughout the relaxation process, including the earliest accessible times. The nonzero N_2 reflects nonaffine deformation of chain segments, even at times well within the retraction regime.

Acknowledgments We gratefully acknowledge financial support from the National Science Foundation, grant CTS-9109898 (Northwestern), and the Amoco Foundation (IIT).

References

Baek SG, Magda JJ, Cementwala S (1993a) Normal stress difference in liquid crystalline hydroxypropylcellulose solutions. J Rheol 37:935–945

Baek SG, Magda JJ, Larson RG (1993b) Rheological differences among liquid-crystalline polymers. I. The first and second normal stress differences of PBG solutions. J Rheol 37:1201–1224

Bernstein B, Feigl KA, Olsen ET (1994) Steady flows of viscoelastic fluids in axisymmetric abrupt conctraction geometry: a comparison of numerical results. J Rheol 38:53–71

Brown EF (1993) Optical characterization of normal stress relaxation in polymers following single-step deformation. MS Thesis, Northwestern University, Evanston

Christiansen EB, Leppard WR (1974) Steady-state and oscillatory flow properties of polymer solutions. Trans Soc Rheol 18:65–86

Doi M (1980) Molecular rheology of concentrated polymer systems. I. J Polym Sci, Polym Phys Ed 18:1005–1020

Doi M, Edwards SF (1986) The theory of polymer dynamics. Oxford University Press, Oxford

Dupont S, Crochet MJ (1988) The vortex growth of a K.B.K.Z. Fluid in an abrupt contraction. J Non-Newt Fluid Mech 29:81–91

Feigl KA, Öttinger, HC (1994) The flow of a LDPE melt through an axisymmetric contraction: a numerical study and comparison to experimental results. J Rheol 39:847–874

Frattini PL, Fuller GG (1984) A note of phase-modulated flow birefringence: a promising rheo-optical method. J Rheol 28:61–70

Rheologica Acta, Vol. 34, No. 3 (1995)

Ginn RF, Metzner AB (1969) Measurement of stresses developed in steady laminar shearing flows of viscoelastic media. Trans Soc Rheol 13:429–453

Goublomme A, Crochet MJ (1993) Numerical prediction of extrudate swell of a high-density polyethylene: further results. J Non-Newt Fluid Mech 47: 281–287

Hassager O (1985) Do polymers really climb rods? J Rheol 29:361–364

Hongladarom K, Burghardt WR (1994) Measurement of the full refractive index tensor in sheared liquid crystalline polymers. Macromolecules 27:483–489

Janeschitz-Kriegl H (1983) Polymer melt rheology and flow birefringence. Springer Verlag, Berlin

Kannan RM, Kornfield JA (1992) The third-normal stress difference in entangled melts – quantitative stress-optical measurements in oscillatory shear. Rheol Acta 31:535–544

Larson RG (1988) Constitutive equations for polymer melts and solutions. Butterworths, Boston

Larson RG, Khan SA, Raju VR (1988) Relaxation of stress and birefringence in polymers of high molecular weight. J Rheol 32:145–161

Larson RG (1992) Instabilities in viscoelastic flows. Rheol Acta 31: 213–263

Leppard WR, Christiansen EB (1975) Transient viscoelastic flow of polymer solutions. AIChE J 21:999–1006

Lodge AS, Meissner J (1972) On the use of instantaneous strains, superposed on shear and elongational flows of polymer liquids, to test the Gaussian network hypothesis and to estimate the segment concentration and its variation during flow. Rheol Acta 11:351–352

Luo XL, Tanner RI (1986) A streamline element scheme for solving viscoelastic flow problems. Part II: Integral constitutive models. J Non-Newt Fluid Mech 22:61–89

Luo XL, Mitsoulis E (1990) A numerical study of the effect of elongational viscosity on vortex growth in contraction flows of polyethylene melts. J Rheol 34:309–342

Magda JJ, Lou J, Baek SG, DeVries KL (1991a) Second normal stress difference of a Boger fluid. Polymer 32: 2000–2009

Magda JJ, Baek SG, DeVries KL, Larson RG (1991b) Shear flows of liquid crystalline polymers: measurements of the second normal stress difference and the Doi molecular theory. Macromolecules 24:4460–4468

Magda JJ, Lee CS, Muller SJ, Larson RG (1993) Rheology, flow instabilities, and shear-induced diffusion in polystyrene solutions. Macromolecules 26: 1696–1706

Magda JJ, Baek SG (1994) Concentrated entangled and semidilute entangled polystyrene solutions and the second normal stress difference. Polymer 35: 1187–1194

Meissner J, Garbella RW, Hostettler J (1989) Measuring normal stress difference in polymer melt shear flow. J Rheol 33:843–864

Miller MJ, Christiansen EB (1972) The stress state of elastic fluids in viscometric flow. AIChE J 18:600–608

Olabisi O, Williams MC (1972) Secondary and primary normal stresses, hole error, and reservoir edge effects in cone-and-plate flow of polymer solutions. Trans Soc Rheol 16:727–759

Osaki K, Kumura S, Kurata M (1981) Relaxation of shear and normal stresses in step-shear deformation of a polystyrene solution. Comparison with the predictions of the Doi-Edwards theory. J Polym Sci: Polym Phys Ed 19:517–527

Osaki K, Nishizawa K, Kurata M (1982) Material time constant characterizing the nonlinear viscoelasticity of entangled polymeric systems. Macromolecules 14:1068–1071

Pearson DS, Kiss AD, Fetters LG, Doi M (1989) Flow-induced birefringence of concentrated polyisoprene solutions. J Rheol 33:517–535

Philippoff W (1961) Experimental tests of symmetry conditions in laminar flow. Trans Soc Rheol 5:149–162

Ramachandran S, Gao HW, Christiansen EB (1985) Dependence of viscoelastic flow functions on molecular structure for linear and branched polymers. Macromolecules 18:695–699

Shaqfeh ESG, Muller SJ, Larson RG (1992) The effects of gap width and dilute solution properties on the viscoelastic Taylor-Couette instability. J Fluid Mech 235:285–317

Soskey PR, Winter HH (1984) Large step shear strain experiments with parallel-disk rotational rheometers. J Rheol 28:625–645

Tanner RI (1970) Some methods for estimating the normal stress functions in viscometric flows. Trans Soc Rheol 14:483–507

Venerus DC, Kahvand H (1994a) Doi-Edwards theory evaluation in double-step strain flows. J Polym Sci, Part B: Polym Phys 32:1531–1542

Venerus DC, Kahvand H (1994b) Normal stress relaxation in reversing double-step strain flows. J Rheol 38:1297–1315

Wagner MH (1994) The origin of the C_2 term in rubber elasticity. J Rheol 38: 655–679

Wales JLS, Philippoff W (1973) The anisotropy of simple shearing flow. Rheol Acta 12:25–34

Walters K (1975) Rheometry. Chapman and Hall, London